Single-particle and collective excitations in ^{63}Ni

M. Albers,[1,*] S. Zhu,[1] R. V. F. Janssens,[1] J. Gellanki,[2] I. Ragnarsson,[3] M. Alcorta,[1] T. Baugher,[4,5] P. F. Bertone,[1,†] M. P. Carpenter,[1] C. J. Chiara,[1,6] P. Chowdhury,[7] A. N. Deacon,[8,‡] A. Gade,[4,5] B. DiGiovine,[1] C. R. Hoffman,[1] F. G. Kondev,[9] T. Lauritsen,[1] C. J. Lister,[1,§] E. A. McCutchan,[1,‖] D. S. Moerland,[1,10] C. Nair,[1] A. M. Rogers,[1,¶] and D. Seweryniak[1]

[1]*Physics Division, Argonne National Laboratory, Argonne, Illinois 60439, USA*
[2]*Department of Physics, Lund University, S-22100 Lund, Sweden*
[3]*Division of Mathematical Physics, LTH, Lund University, S-22100 Lund, Sweden*
[4]*National Superconducting Cyclotron Laboratory, Michigan State University, East Lansing, Michigan 48824, USA*
[5]*Department of Physics and Astronomy, Michigan State University, East Lansing, Michigan 48824, USA*
[6]*Department of Chemistry and Biochemistry, University of Maryland, College Park, Maryland 20742, USA*
[7]*Department of Physics, University of Massachusetts, Lowell, Massachusetts 01854, USA*
[8]*School of Physics and Astronomy, Schuster Laboratory, University of Manchester, Manchester M13 9PL, United Kingdom*
[9]*Nuclear Engineering Division, Argonne National Laboratory, Argonne, Illinois 60439, USA*
[10]*Department of Physics, Florida State University, Tallahassee, Florida 32306, USA*

(Received 6 September 2013; published 18 November 2013)

A study of excited states in ^{63}Ni up to an excitation energy of 28 MeV and a probable spin of 57/2 was carried out with the ^{26}Mg(^{48}Ca,2α3$n\gamma$)^{63}Ni reaction at beam energies between 275 and 320 MeV. Three collective bands, built upon states of single-particle character, were identified. For two of the three bands, the transition quadrupole moments were extracted, herewith quantifying the deformation at high spin. The results have been compared with shell-model and cranked Nilsson-Strutinsky calculations. Despite the $Z = 28$ shell closure and the approach to the purported $N = 40$ subshell, the ^{63}Ni isotope is able to sustain collective excitations at moderate and high spin.

DOI: 10.1103/PhysRevC.88.054314 PACS number(s): 21.60.Cs, 21.10.Ky, 23.20.En, 27.50.+e

I. INTRODUCTION

Neutron-rich nuclei in the $A \approx 60$ mass region have been the subject of many recent experimental and theoretical investigations. Specifically, much attention has been devoted to documenting the evolution of shell structure with neutron number N in nuclei located above doubly-magic ^{48}Ca. In neutron-rich ^{52}Ca [1], ^{54}Ti [2], and ^{56}Cr [3], a new subshell gap was established at $N = 32$, based on systematic studies of 2_1^+ energies and $B(E2;2_1^+ \rightarrow 0_1^+)$ transition strengths [4–7]. Indications of an $N = 34$ subshell closure have been found in ^{54}Ca [8]. It is by now well established that the monopole part of the tensor force plays a central role in the development of these two gaps [9–12]. In contrast, in neutron-rich nuclei between $Z = 20$ and $Z = 28$ close to the proton mid-shell, evidence of sizable collectivity at low and medium spin has been accumulating. In both the Cr and Fe isotopic chains, the energies of the 2_1^+ and 4_1^+ states decrease as N increases towards $N = 40$ [13,14], culminating in the 2_1^+ energy in ^{64}Cr being the lowest among all the known $N = 40$ isotones [13]. Lifetime information and $B(E2;2_1^+ \rightarrow 0_1^+)$ transition strengths for ^{58,60,62,64}Cr [15,16] and ^{62,64,66,68}Fe [14,16,17] constitute additional supporting evidence. Furthermore, level sequences of rotational character have been reported at high spin in the Cr, Mn, and Fe isotopic chains [4,18–22]. These observations have led Carpenter *et al.* [23] to propose a shape-coexistence picture to describe the low- and medium-spin structure of the even, neutron-rich Cr and Fe isotopes. Also, shell-model calculations have pointed to the importance of the deformation-driving $\nu 0g_{9/2}$ and $\nu 1d_{5/2}$ orbitals in this context [18,24,25].

In the Ni isotopic chain, the $Z = 28$ shell closure stabilizes a spherical shape near the ground state in nuclei between ^{56}Ni and ^{78}Ni and the level sequences at low and moderate spin are described well by shell-model calculations [26]. Here, the filling of the neutron $p_{3/2}$, $f_{5/2}$, $p_{1/2}$, and $g_{9/2}$ orbitals determines mostly the structure of low-energy excitations as shown quantitatively in the study of Ref. [27]. An $N = 40$ subshell closure is visible in ^{68}Ni through (i) the presence of a 0_2^+ state as the lowest excitation [28], (ii) the fact that the 2_1^+ level is located at a high energy and is characterized by a small $B(E2;2_1^+ \rightarrow 0_1^+)$ strength [26,29], and (iii) the occurrence of a long-lived 5^- isomer [26,30]. However, this $N = 40$ gap between the $p_{1/2}$ and $g_{9/2}$ single-particle states is estimated to be of the order of only 2 MeV. This relatively small value supports the results of shell-model calculations reproducing the structure of the yrast and near-yrast excited states in "doubly-magic" ^{68}Ni and in its one-hole neighbor ^{67}Ni which indicate that all the yrast and near-yrast levels are associated with complex configurations involving cross-shell excitations [26,31].

*malbers@phy.anl.gov
†Present address: Marshall Space Flight Center, Building 4600 Rideout Rd, Huntsville, Alabama 35812, USA.
‡Present address: Cargo Division, Rapiscan Systems, Stocke-on-Trent ST8 7PL, United Kingdom.
§Present address: Department of Physics, University of Massachusetts, Lowell, Massachusetts 01854, USA.
‖Present address: National Nuclear Data Center, Brookhaven National Laboratory, Upton, New York 11973-5000, USA.
¶Present address: Nuclear Science Division, Lawrence Berkeley National Laboratory, Berkeley, California 94720, USA.

Rotational sequences have been reported at moderate and high spin in some of the lighter even-even Ni isotopes: highly deformed and even superdeformed bands, built upon lower-lying single-particle excitations, have been observed in doubly-magic ^{56}Ni [32,33], as well as in ^{57}Ni [34,35], ^{58}Ni [36–38], ^{59}Ni [39], and ^{60}Ni [40,41]. Remarkably, partial proton and alpha decays out of some of these bands have been reported in ^{56}Ni and ^{58}Ni. In contrast, no experimental evidence for collective excitations has been reported thus far for Ni isotopes closer to the $N = 40$ subshell closure. This is, at least in part, due to difficulties in producing these nuclei at the required high spins with conventional fusion-evaporation reactions because of the lack of suitable projectile-target combinations.

The present work reports on a new investigation of the ^{63}Ni nucleus, populated in a complex, high-energy reaction ^{26}Mg(^{48}Ca,$2\alpha 3n\gamma$) carried out in inverse kinematics. The use of a heavy beam on a lighter target provides the opportunity to perform coincidence measurements between γ rays and reaction products with full isotopic identification (e.g., mass A and charge Z). As a result, the existing low-spin sequence of single-particle states in ^{63}Ni [42,43] was significantly expanded. More importantly, three rotational bands were discovered, of which two were linked to the lower-spin levels, herewith enabling the assignment of spin and parity quantum numbers within the sequences. Transition quadrupole moments were also extracted for two of the bands from partial Doppler shifts, albeit with rather large uncertainties. For the lower-spin states, the data are compared with the results of shell-model calculations in an $f_{5/2}pg_{9/2}$ model space while the rotational bands are interpreted with guidance from calculations within the cranked Nilsson-Strutinsky approach.

II. EXPERIMENT

A novel experimental approach was used in an attempt to produce a large number of neutron-rich nuclei at high spin using complex reactions in inverse kinematics. A ^{48}Ca beam was provided by the Argonne Tandem Linac Accelerator System (ATLAS) at Argonne National Laboratory and impinged upon a self-supporting, 0.973-mg/cm^2-thick ^{26}Mg target. The beam energies of 275, 290, and 320 MeV were chosen to be roughly 200% above the Coulomb barrier in order to favor multi-nucleon transfer processes in inverse kinematics [44]. The target was placed in the center of the Gammasphere array [45], comprising 101 Compton-suppressed high-purity germanium (HPGe) detectors. The energy and efficiency for each HPGe detector was calibrated using standard ^{56}Co, ^{152}Eu, ^{182}Ta, and ^{243}Am sources.

The reaction products were transported through the Argonne Fragment Mass Analyzer (FMA) [46] and were dispersed at the focal plane of the instrument according to their mass-to-charge ratio, M/q. However, in order to match the energy acceptance of the FMA, the recoil energy was degraded by placing a 0.7-mg/cm^2-thick $^{\text{nat}}$Ti foil directly in front of the entrance quadrupole, well outside the focus of Gammasphere. The use of this degrader did neither noticeably affect the position resolution at the focal plane nor cause an observable broadening of the recoil-particle cone. A microchannel plate (MCP) detector provided the position information for each recorded particle from which the corresponding M/q value was derived. For the Z identification, a threefold segmented ionization chamber, operated at 25 Torr, was placed 50 cm behind the focal plane. The first two segments, each of 5 cm length, were used to measure the energy loss of the products. The recoils came to rest in the third segment with a length of 20 cm. The trigger logic required the detection of a reaction product in the MCP detector in coincidence with a minimum of two γ rays in Gammasphere. For all events, the associated time information was recorded as well, thus enabling the measurement of the time of flight, *ToF*, of the transported reaction residues from the target to the FMA focal plane as well as the sorting of γ rays into various coincidence histograms with an appropriate prompt time condition.

Typical particle-identification plots are provided in Figs. 1(a)–1(c). In the top panel, the energy loss in the first two segments of the ionization chamber, ΔE, is plotted against the total energy (i.e., the sum of all three segments of the ionization chamber) of the products E_{total}. Unit Z separation is achieved, and the circled region in the figure corresponds to the Ni isotopes. In Fig. 1(b), the product of the total energy and the flight time ET^2 is displayed as a function of the charge-to-mass ratio M/q for the Ni isotopes. Despite achieving the desired separation between various products, ambiguities in M/q are present which made it imperative to implement an additional coincidence gate in the two-dimensional histogram of *ToF* versus E_{total} [see Fig. 1(c)]. A combination of the three coincidence conditions was subsequently implemented in the analysis to generate γ-γ coincidence matrices.

Figure 2(a) presents the total projection of the γ-γ coincidence matrix for ^{63}Ni obtained by placing gates on the focal-plane information described above. Transitions belonging to the low-energy level structure (labeled $ND1$ in the discussion hereafter) are indicated by their respective energies. While most of the γ rays could be readily associated with ^{63}Ni, care was taken to identify possible contaminants from other reaction channels by inspecting numerous spectra in coincidence with the strongest transitions in these other nuclei. The panels (b), (c), and (d) of the figure present representative coincidence spectra for three long γ-ray cascades identified in the present work. In each case, the energies of the relevant γ rays are given and the histograms have been obtained by summing the coincidence data for all in-band transitions. The resulting sequences of levels are labeled $D1$, $D2$, and $D3$ in the level scheme of Fig. 3.

Spin and parity assignments are based mainly on examining the observed decay patterns and on analyzing either angular distributions (ADs) [47] and/or angular-correlation (AC) ratios (R_{AC}) [48] of deexciting γ rays. Comparisons with shell-model calculations (see below) were also taken into account. As the ADs are symmetric around 90°, detectors at corresponding angles with respect to the beam axis in the forward and backward hemispheres were combined into a total of seven average laboratory angles between 17.3° and 90.0°. Gamma-ray intensities were determined for each angle and fitted to the canonical AD expression $W(\Theta) = a_0[1 + a_2P_2(\cos\Theta) + a_4P_4(\cos\Theta)]$, where P_n are the Legendre polynomials of the

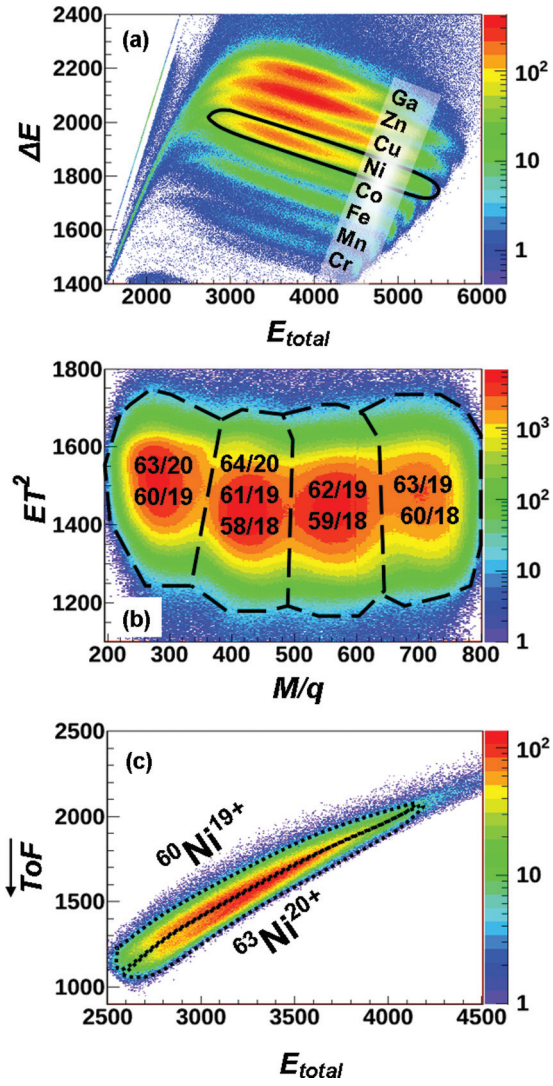

FIG. 1. (Color online) Two-dimensional particle identification plots: (a) ΔE vs E_{total} histogram with different element groups labeled. The solid contour line indicates the particle gate for Z selection. (b) ET^2 vs M/q histogram of the detected ions obtained after Z selection. The dashed lines indicate the particle gates for the M/q selection; note the M/q ambiguities. (c) ToF vs E_{total} plot following Z and M/q selection used to resolve the ambiguity in M/q. The dotted lines indicate particles with the same M/q ratio, but different masses M. All axes are in arbitrary units.

nth order, and the a_2 and a_4 coefficients contain the information on the multipolarity of the transition. In order to extract the AC ratios R_{AC}, two coincidence matrices were incremented. The first such matrix [referred to as $M(0^\circ, any)$ hereafter] required γ rays observed in detectors with angles 31.7°, 37.4°, 142.6°, 148.3°, and 162.7° to be placed on one axis, with coincident transitions measured at any angle grouped along the other. The second matrix [$M(90^\circ, any)$] was similar, but with detectors with angles 79.2°, 80.7°, 90.0°, 99.3°, and 100.8° on the one axis. The AC ratio is then defined as $R_{\text{AC}} = \frac{I_\gamma(M(0^\circ,any))}{I_\gamma(M(90^\circ,any))}$, where $I_\gamma(M(X, any))$ denotes the intensity of a γ ray detected in the *ad hoc* matrix. Coincidence gates were placed on transitions of stretched-quadrupole character only. For a sequence of two quadrupole γ rays (Q–Q), an AC ratio of $R_{\text{AC}} > 1$ is expected, while a stretched-quadrupole-dipole sequence (Q–D) results in $R_{\text{AC}} < 1$. In the case of a sequence with a stretched-quadrupole and a mixed-dipole-quadrupole (Q–D/Q) γ ray, R_{AC} depends on the magnitude and the sign of the multipole mixing ratio δ. This can introduce some ambiguity and result in tentative spin-parity assignments. A summary of the relevant experimental information in terms of level and γ-ray properties can be found in Table I.

The thin-target, Doppler-shift-attenuation method was employed to extract, albeit with larger errors, transition quadrupole moments for a limited number of transitions in the $D1$ and $D2$ bands, following the method of Ref. [49]. Despite the use of a thin target, a number of transitions in the cascades of interest were emitted before the residues escaped the target; i.e., while the recoiling nuclei are slowing down in the material. As a result, these γ rays exhibit Doppler shifts different from the average one and a fractional shift $F(\tau)$ can be deduced from spectra measured at different angles. This procedure was followed to obtain $F(\tau)$ values from the $E_{\text{beam}} = 320$ MeV data. The relevant $F(\tau)$ values are plotted versus transition energies for bands $D1$ and $D2$ in Figs. 4(a) and 4(b), respectively. Transition quadrupole moments Q_T were extracted from comparisons with simulated $F(\tau)$ fractions computed with the Monte Carlo code WLIFE4 [50]. The latter follows the emission of γ rays emitted by recoiling nuclei decelerating in the target. The stopping process was obtained from the SRIM2008 computer code [51]. Side-feeding transitions were considered by means of a single rotational cascade with the same dynamic moment of inertia $\mathcal{J}^{(2)}$ and the same transitional quadrupole moment Q_T as the sequence under analysis. An additional parameter T_{SF} accounts for a one-step feeding delay on top of each band and was set to $T_{\text{SF}} = 1$ fs throughout the analysis. A χ^2 minimization was carried out. The best fit is indicated by the solid black lines in Fig. 4. The statistical errors $\Delta F(\tau)_{\text{stat}}$, obtained from fits with a χ^2 value increased by one, result in the dashed blue lines of Fig. 4. In addition, a systematic error of $\Delta F(\tau)_{\text{sys}} = \pm 10\%$ is added to take uncertainties in the simulation of the stopping process into account.

III. RESULTS

A total of 38 excited states, feeding the $9/2^+$ isomer ($t_{1/2} = 3.3$ ns [42]) either directly or indirectly, were placed in the level scheme of ^{63}Ni on the basis of the coincidence analysis discussed above. The construction of the level scheme started from the earlier work of Refs. [42,43], and just above the long-lived state, a number of levels have been grouped under the label $ND1$ in Fig. 3. For these levels, firm spin and parity assignments are proposed on the basis of the measured angular distributions and correlations (see Table I). All the transitions associated with the $ND1$ sequence were found to be characterized by the average Doppler shift; i.e., the associated feeding and intrinsic state lifetimes are longer than the time taken by the ^{63}Ni nuclei to escape the target.

Band $D1$ extends from the $17/2^+$ level at 4871 keV to the $(53/2^+)$ state at 24 499 keV. This sequence is unambiguously linked to the $ND1$ structure via two depopulating γ-ray

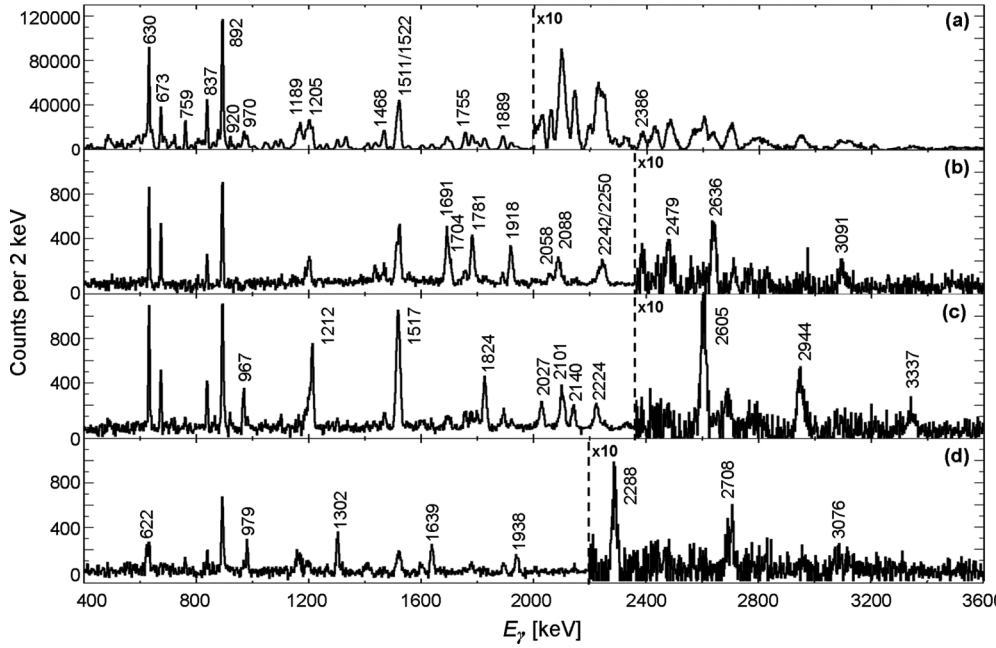

FIG. 2. Background-subtracted coincidence spectra with gates on ^{63}Ni recoils detected in the FMA. (a) Total projection of the full γ-γ matrix for ^{63}Ni; transitions belonging to the low-energy structure (referred to in the text as $ND1$) are labeled with their respective energies. (b)–(d) Sum of coincidence gates on in-band γ-ray transitions in the three collective bands labeled $D1$ (b), $D2$ (c), and $D3$ (d) in the text. The γ rays of interest are indicated by their energies.

transitions of 2058 and 2250 keV, and the spin and parity of the bandhead are firmly established as $17/2^+$ from the AD and AC data. Higher-lying levels within band $D1$ are connected via a cascade of transitions with stretched-$E2$ character. Only for the highest-spin state was a multipolarity determination not possible due to weak feeding, and the $53/2^+$ spin and parity quantum numbers are proposed on the basis of the natural extension of a band of rotational character. As discussed in the previous section, $F(\tau)$ values were obtained for some of the transitions and an analysis with the WLIFE4 code was carried out. A transition quadrupole moment of $Q_T = 2.4^{+1.7}_{-1.2}$ eb was derived, which translates into a value of $|\beta_2| = 0.43^{+0.25}_{-0.20}$ for the quadrupole deformation parameter.

Band $D2$ is the most intense of the three sequences, as illustrated in Fig. 5, where intensities are presented as a function of the γ-ray energies. As a result, it also contains the highest excitation (27 223 keV) observed in the present work and is, hence, assumed to be yrast at high angular momentum. A single 967-keV transition was found to link the $D2$ and $ND1$ level structures. This γ ray is weaker than the lowest in-band transitions (Table I), indicating that the deexcitation out of the band proceeds through more than one path. This finding is confirmed by the coincidence spectra gated on both the in-band and $ND1$ transitions, but it was not possible to delineate additional paths due, presumably, to a degree of fragmentation of the missing intensity. The angular-distribution information for the 967-keV γ ray limits the spin-parity of the bandhead to $17/2^{\pm}$, $19/2^+$, or $21/2^+$. Comparisons with the results from cranked Nilsson-Strutinsky model calculations presented in the next section lead to the proposed, tentative $I^\pi = 17/l; 2^+$ values. The in-band transitions exhibit a stretched-$E2$ character, except for the highest one, where the limited statistics did not allow the extraction of an angular distribution and the tentative spin-parity assignment is proposed based on the extension of a sequence of quadrupole γ rays. As was the case for band $D1$, the transitional quadrupole moment was obtained from the $F(\tau)$ values of a few transitions. The relevant fit is presented together with the data in Fig. 4 and the corresponding moment has the value $Q_T = 1.9^{+1.3}_{-1.2}$ eb which translates into a quadrupole deformation parameter of $|\beta_2| = 0.35^{+0.20}_{-0.21}$.

An additional sequence of stretched-$E2$ transitions, labeled $D3$, was also observed in the present measurement. As can be seen from Fig. 5 and Table I, it is characterized by an intensity roughly a factor of 3 smaller than that of bands $D1$ and $D2$. While the assignment to ^{63}Ni is confirmed through the observed coincidence relationships and the gating on the A and Z information measured at the FMA focal plane, the precise excitation energy of band $D3$ remains in doubt, as illustrated in the level scheme of Fig. 3. The available evidence indicates that the cascade feeds mostly into the $21/2^-$ state at 6.3 MeV of the $ND1$ structure, suggesting a likely negative parity for the states within band $D3$. However, at the bottom of the sequence, the 622-keV line appears to be somewhat less intense than the preceding 979- and 1302-keV γ rays, a situation not without similarity to that observed in the decay out of superdeformed bands [52]. Furthermore, the assumption that the 622-keV transition is a direct link to the $21/2^-$ level would lead to the conclusion that band $D3$ is yrast over most of the observed spin range, in contradiction with the measured relative intensities of the three bands. It is, thus, likely that the deexcitation proceeds through a number of linking transitions of intensity below the detection sensitivity of the experiment, as is sometimes the case with superdeformed and other collective bands. Figure 5

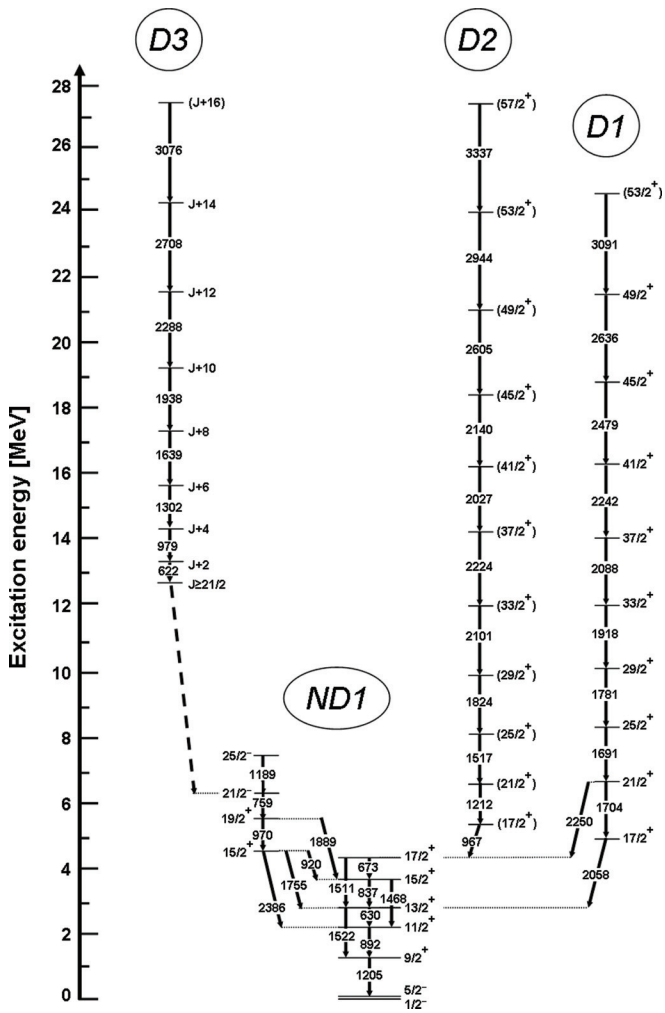

FIG. 3. Level scheme of ^{63}Ni deduced in the present work. The states are labeled with their spins and parities.

also indicates that the intensity of band $D1$ becomes similar to those of the two other bands at the highest transition energies. The assumption that this observation can be related with the fact that, at the highest spins, the three bands are close in excitation energy and, hence, compete for yrast status, leads to a rough estimate of the excitation energy and spin of the bandhead illustrated in Fig. 6. If the highest level of band $D3$ lies close in energy to the $(57/2^+)$ state in band $D2$, as indicated in the figure, the bandhead would be characterized by an excitation energy of about 12.7 MeV and a spin value of $25/2$. These two quantities become 9.95 MeV and $21/2$ when the highest levels of bands $D1$ and $D3$ are closest in energy (not shown in Fig. 6). Note that these conjectures do not imply that the sequence is necessarily characterized by a large deformation: due to low statistics, it was not possible to extract a transition quadrupole moment for band $D3$.

By examining Figs. 5 and 6, both the intensity pattern of the three bands and their decay-out behavior can be readily understood. For bands $D1$ and $D2$, the intensities increase with decreasing spin due to the fact that they are fed from higher-lying states over nearly the entire sequence of observed levels. This suggests that these bands are yrast or near-yrast over their entire range. It then follows that, at the point of decay to the $ND1$ states, the number of levels available for the bands to decay into is rather small, resulting in the observation of linking transitions. In contrast, Fig. 6 indicates that band $D3$ quickly becomes non-yrast, consistent with the observation that the band is only fed at the highest spins. In addition, at the point of decay, the band lies high in excitation energy which should result in sizable fragmentation of the decay to the $ND1$ states as has been observed for superdeformed bands.

IV. DISCUSSION

A. Collectivity and deformation in ^{63}Ni

As discussed above, three sequences with rotational character ($D1$, $D2$, and $D3$) are present at fairly low spin and excitation energy in ^{63}Ni. In Fig. 7(a), the evolution with rotational frequency, ω, of the spin along the rotational axis, I_x, for the three bands is compared with that observed in Ref. [21] for the yrast sequence of ^{60}Fe. Note that the spin vector is assumed to be directed along the x axis, i.e., $I_x = I$. Above $I^\pi = 6^+$, the levels of the yrast sequence of ^{60}Fe have been interpreted in terms of a rotational band with an aligned pair of $g_{9/2}$ neutrons which is associated with an axially symmetric nuclear shape and a deformation parameter $\beta_2 \sim 0.2$. At frequencies below 1 MeV/$\hbar$, the states in bands $D1$ (solid red squares) and $D2$ (solid blue triangles) exhibit I_x values comparable to those of the $\nu(g_{9/2})^2$ configuration in ^{60}Fe, suggesting that the excitations are of the same character and are associated with a deformed shape as well. At higher frequencies, however, an additional gain in I_x is visible in bands $D1$ and $D2$. While the increase is smooth in the $D1$ sequence, it is sudden in band $D2$: a backbending occurs around $I = 41/2$, indicative of a band crossing and a change in intrinsic structure that is discussed in the next section. For illustration purposes, band $D3$ (solid green circles) is plotted in the figure under the assumptions discussed above and represented in Fig. 6; i.e., with a bandhead energy of 12.7 MeV and a spin value of $25/2$. The resulting trajectory in the I_x vs ω plane is similar to those of the two other sequences at higher rotational frequencies ($\omega > 1$ MeV/$\hbar$). Thus, the data support the view that deformation is present and also suggest that the three bands are associated with configurations involving the alignment of several particles with the rotational axis.

Further information on the nature of the three sequences can be gathered from comparisons with other deformed bands in nuclei of the $A = 60$ mass region. Figure 7(b) illustrates the angular momentum gain I_x vs rotational frequency for selected bands in ^{56}Ni ($SD2$ in [32,33]), ^{57}Ni ($SD1$ in [34,35]), ^{58}Ni ($B3$ in [37]), ^{59}Ni ($B2$ in [39]), and ^{60}Ni ($WD2$ in [41]): all are close to the trajectory of the $\nu(g_{9/2})^2$ excitation in ^{60}Fe. In fact, configurations assigned to the respective bands in $^{57-60}$Ni include at least two particles (protons and/or neutrons) in the $g_{9/2}$ orbitals while, for band SD2 in ^{56}Ni, the configuration involves a single $g_{9/2}$ proton. For these five sequences, the deformation parameter $|\beta_2|$ was either obtained from a lifetime measurement or inferred from comparisons of the data with cranked Nilsson-Strutinsky calculations (see Table II). The reported $|\beta_2|$ values are of the order of 0.3 or larger; i.e., in the

TABLE I. Summary of the experimental results on ^{63}Ni: level energies E_x, spin and parity of the initial (i) and the final (f) states $I^\pi_{i,f}$, transition energies E_γ and efficiency-corrected relative intensities I_γ of deexciting γ rays, Legendre coefficients a_2 and a_4 deduced from the angular-distribution analysis, angular-correlation ratios $R_{\rm AC}$, and multipolarity $\sigma\lambda$.

E_x (keV)	I^π_i ($\hbar$)	I^π_f ($\hbar$)	E_γ (keV)	I_γ	a_2	a_4	$R_{\rm AC}$	$\sigma\lambda$
*ND*1								
1291.8(2)	$9/2^+$	$5/2^-$	1204.7(1)		0.39(1)	−0.07(3)	1.33(7)	$M2/E3$
2183.3(3)	$11/2^+$	$9/2^+$	891.5(1)	936(28)	0.15(1)	−0.14(1)	1.24(6)	$M1/E2$
2813.5(4)	$13/2^+$	$11/2^+$	630.1(1)	1000(34)	−0.07(3)	−0.07(4)	1.07(3)	$M1/E2$
		$9/2^+$	1521.9(4)	400(23)	0.17(1)	−0.19(2)	0.96(7)	$E2$
3650.4(5)	$15/2^+$	$13/2^+$	836.8(1)	711(27)	0.03(2)	−0.21(3)	1.24(5)	$M1/E2$
		$11/2^+$	1467.6(3)	237(27)	0.21(5)	−0.23(6)	1.27(7)	$E2$
4323.4(5)	$17/2^+$	$15/2^+$	672.8(1)	605(25)	−0.13(1)	0.01(1)	0.93(4)	$M1/E2$
		$13/2^+$	1510.8(3)	248(18)	0.00(28)		0.81(7)	$E2$
4569.7(6)	$15/2^+$	$15/2^+$	919.9(2)	263(12)	0.06(5)		1.12(8)	$M1/E2$
		$13/2^+$	1755.4(2)	375(12)	0.07(3)	−0.14(4)	1.59(12)	$M1/E2$
		$11/2^+$	2385.7(5)	44(12)				$E2$
5539.3(6)	$19/2^+$	$15/2^+$	969.7(3)	199(18)	0.15(2)	−0.19(3)	1.09(11)	$E2$
		$15/2^+$	1888.9(2)	381(16)	0.04(2)	−0.19(3)	1.21(7)	$E2$
6298.6(7)	$21/2^-$	$19/2^+$	759.3(1)	444(10)	−0.21(1)	0.02(2)	0.75(9)	$E1$
7487.6(8)	$25/2^-$	$21/2^-$	1189.0(2)	392(12)	0.04(4)	−0.22(6)	1.48(13)	$E2$
*D*1								
4871.1(10)	$17/2^+$	$13/2^+$	2058.3(4)	117(16)	0.41(12)	−0.15(15)	1.13(19)	$E2$
6573.5(8)	$21/2^+$	$17/2^+$	1703.5(4)	74(15)	0.02(8)	0.00(11)	1.72(15)	$E2$
		$17/2^+$	2249.9(2)	168(31)	0.31(4)	−0.13(5)	1.21(13)	$E2$
8265.3(9)	$25/2^+$	$21/2^+$	1690.9(2)	214(35)	0.15(8)	−0.22(11)	1.31(8)	$E2$
10045.1(10)	$29/2^+$	$25/2^+$	1780.8(2)	209(33)	0.18(2)	−0.27(3)	1.52(9)	$E2$
11963.0(12)	$33/2^+$	$29/2^+$	1917.9(2)	174(26)	0.10(6)	0.18(9)	1.01(8)	$E2$
14050.5(14)	$37/2^+$	$33/2^+$	2087.6(3)	161(22)	0.12(4)	−0.32(6)	1.37(14)	$E2$
16292.5(15)	$41/2^+$	$37/2^+$	2241.9(5)	168(31)			1.24(18)	$E2$
18771.2(28)	$45/2^+$	$41/2^+$	2478.8(21)	11(11)	0.49(9)	−0.06(12)	2.25(39)	$E2$
21407.4(46)	$49/2^+$	$45/2^+$	2636.2(12)	17(11)	0.57(34)		1.95(24)	$E2$
24498.8(70)	$(53/2^+)$	$49/2^+$	3091.4(18)	<5				
*D*2								
5290.5(6)	$(17/2^+)$	$17/2^+$	967.1(2)	161(31)	0.14(6)		1.43(21)	$E2$
6501.9(7)	$(21/2^+)$	$(17/2^+)$	1211.5(2)	362(31)	0.09(8)	0.33(10)	1.50(11)	$E2$
8019.2(8)	$(25/2^+)$	$(21/2^+)$	1517.2(2)	331(44)	0.11(6)	−0.40(8)	1.50(7)	$E2$
9843.5(9)	$(29/2^+)$	$(25/2^+)$	1824.4(2)	264(24)	0.15(20)		1.51(10)	$E2$
11944.9(10)	$(33/2^+)$	$(29/2^+)$	2101.4(2)	235(22)	0.47(22)	−0.43(28)	1.76(15)	$E2$
14169.3(13)	$(37/2^+)$	$(33/2^+)$	2224.4(3)	124(20)			1.52(23)	$E2$
16196.6(15)	$(41/2^+)$	$(37/2^+)$	2027.3(2)	133(17)	0.23(9)	−0.55(12)	1.21(19)	$E2$
18336.1(17)	$(45/2^+)$	$(41/2^+)$	2139.5(3)	89(13)	0.53(42)		1.66(29)	$E2$
20941.5(21)	$(49/2^+)$	$(45/2^+)$	2605.4(4)	65(13)	0.55(22)		0.94(14)	$E2$
23885.1(41)	$(53/2^+)$	$(49/2^+)$	2943.6(12)	15(9)			1.02(18)	$E2$
27222.5(55)	$(57/2^+)$	$(53/2^+)$	3337.4(13)	<5				
*D*3								
X	$J \geqslant 21/2^{(-)}$	$21/2^-$						
$X + 621.6(9)$	$J+2$	$J \geqslant 21/2^{(-)}$	621.6(4)	76(17)			1.32(15)	$E2$
$X + 1600.4(13)$	$J+4$	$J+2$	978.8(3)	87(17)	0.22(6)	−0.21(8)	1.37(12)	$E2$
$X + 2901.9(15)$	$J+6$	$J+4$	1301.5(3)	94(16)	0.45(12)		1.11(8)	$E2$
$X + 4541.0(21)$	$J+8$	$J+6$	1639.2(5)	55(15)	0.47(12)	−0.30(15)	1.55(13)	$E2$
$X + 6478.7(26)$	$J+10$	$J+8$	1937.6(5)	50(13)	0.00(13)	−0.53(18)	1.46(12)	$E2$
$X + 8766.7(37)$	$J+12$	$J+10$	2288.1(9)	22(11)	0.36(15)	−0.31(20)	1.38(26)	$E2$
$X + 11474.7(56)$	$J+14$	$J+12$	2708.0(14)	13(9)			1.56(27)	$E2$
$X + 14550.2(62)$	$J+16$	$J+14$	3075.5(14)	<5				$E2$

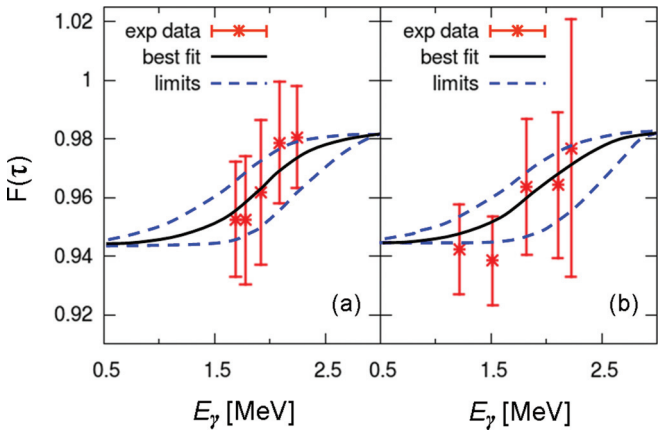

FIG. 4. (Color online) Experimental (points) and calculated (lines) values of the fractional Doppler shift $F(\tau)$ as a function of E_γ for band $D1$ (a) and band $D2$ (b) in ^{63}Ni. The best calculated fit is represented by a solid black line, while the dashed blue lines indicate the statistical errors.

same range as those reported above for bands $D1$ and $D2$ in ^{63}Ni (see Sec. III).

Figure 7(c) extends the I_x vs ω comparison further with selected bands in ^{60}Zn (SD in [53]), ^{61}Zn (SD in [54]), ^{62}Zn (SD in [55] and $SD1$ in [56]), and ^{65}Zn ($SD1$ in [52]). Since the ^{65}Zn $SD1$ band has not yet been firmly linked to the lower-lying states, the spin value of 33/2 proposed by Yu *et al.* [52] for the bandhead was adopted. In comparison with the trajectory for the aligned ($g_{9/2}$) neutrons, these bands exhibit the larger alignment gains that characterize bands $D1$, $D2$, and $D3$ at the highest frequencies. As seen in Table II, the $|\beta_2|$ deformation parameters are available for these bands in the Zn isotopic chain from lifetime measurements carried out with the same Doppler-shift-attenuation method used in the present work. These Zn bands are characterized by $|\beta_2|$ values of 0.4 or higher which lead to an interpretation in terms of superdeformation. Albeit with fairly large uncertainties, the deformation parameters of bands $D1$ and $D2$ in ^{63}Ni appear to be in the same range, suggesting sizable deformation in this case as well.

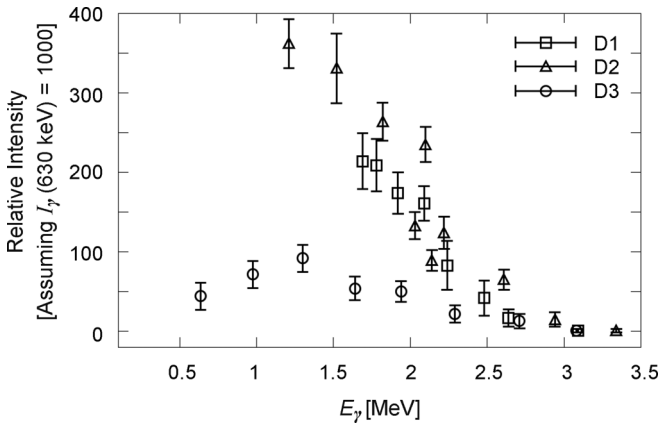

FIG. 5. Intensities of the three observed rotational bands in ^{63}Ni vs the γ-ray transition energy.

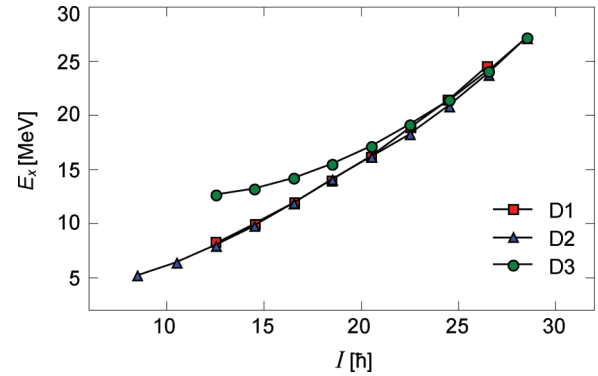

FIG. 6. (Color online) Excitation energy vs spin for the three collective bands observed in the present measurement. The figure is drawn under the assumption that the three bands are very close in excitation energy at the highest spins. This approach provides a means to estimate the bandhead energy and spin of band $D3$ which is not linked to the lower-spin level structure. See text for details.

B. Interpretation from cranked Nilsson-Strutinsky calculations

From the discussion above, it is clear that an interpretation within the framework adopted for the description of most of the collective bands observed in the Ni [32,33,35,37,39,41] and Zn [52–56] isotopic chains is warranted. Hence, calculations were performed within the configuration-dependent cranked Nilsson-Strutinsky (CNS) model with the formalism described in Refs. [57–59]. This model considers rotation from the intrinsic frame of reference, in which nucleons experience the effects of the Coriolis and centrifugal forces. At each spin, the total energy of specific configurations is minimized with respect to the relevant deformation parameters. The calculations have been performed with the single-particle parameters that have recently been fitted [60] to the high-spin bands of nuclei with $A = 56$–62. For the active $\mathcal{N} = 3{,}4$ major shells, these parameters are given in Table III. Pairing effects are neglected as they are expected to play a minor role at high spin ($>15\hbar$). Proton and neutron excitations across the $Z = N = 28$ shell gaps into the $\mathcal{N} = 3{,}4$ orbitals and into the $1g_{9/2}$ orbital are considered, and the configurations of interest are labeled hereafter as $[p_1(\pm)p_2, n_1(\pm)n_2]$, a notation that defines the occupation of active high-j subshells. Here, p_1 (n_1) denotes the number of holes in the $1f_{7/2}$ orbital and p_2 (n_2) denotes the number of particles in the $1g_{9/2}$ orbital for protons (neutrons) relative to a closed ^{56}Ni core [58]. In addition, the ($\pm$) notation is added for an odd number of (fp) protons or neutrons in order to specify the signature of these particles, where (fp) refers to the orbitals of $p_{3/2}f_{5/2}$ character [60].

Results of the CNS calculations and comparisons with the data are displayed in Fig. 8: panel (a) presents the experimental level energies as a function of the angular momentum I with a rotating liquid drop (rld) energy subtracted [59], and panel (b) provides the same energy differences for the bands resulting from the calculations. In Fig. 8(c), the difference between experimental and calculated energies is given, where good agreement between theory and experiment should result in values close to zero. However, because pairing is neglected in the calculations, differences near zero should be expected only

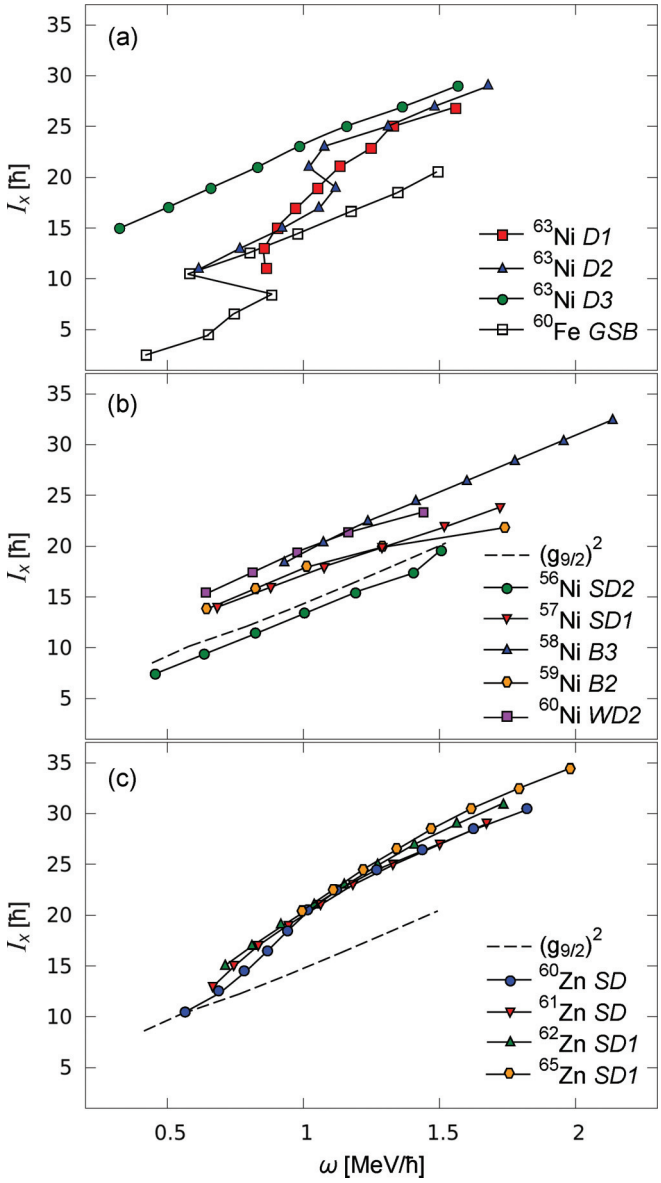

FIG. 7. (Color online) Spin along the rotational axis I_x vs rotational frequency ω for (a) bands $D1$, $D2$, and $D3$ in ^{63}Ni and the ground-state band in ^{60}Fe (*GSB* in [21]); (b) selected rotational bands in ^{56}Ni ($SD2$ in [32,33]), ^{57}Ni ($SD1$ in [34,35]), ^{58}Ni ($B3$ in [37]), ^{59}Ni ($B2$ in [39]), and ^{60}Ni ($WD2$ in [41]) together with the trajectory of the yrast band in ^{60}Fe in the $I = 8$–20 range, where this sequence is associated with a configuration with two aligned $g_{9/2}$ neutrons; (c) same as (b), but for selected bands in ^{60}Zn (SD in [53]), ^{61}Zn (SD in [54]), ^{62}Zn (SD in [55] and $SD1$ in [56]), and ^{65}Zn ($SD1$ in [52]). See text for details.

at high spin, with an increase at lower I values reflecting the gradual gain in importance of pairing with decreasing spin.

As the I^π quantum numbers for the levels in band $D1$ are firmly established, comparisons between experiment and theory are expected to be particularly relevant in this case. In the high-spin range, above $I \approx 20$, the $(E_{\rm exp} - E_{\rm rld})$ curve exhibits a positive curvature: this is typical for unpaired configurations and corresponds to an approximate straight line in the I_x vs ω plane [see Fig. 7(a)]. At lower spins, on the other hand, the curvature is negative and the I_x vs ω curve suggests the presence of one or several alignments. Therefore, it is only at high spin that an assignment to a CNS configuration can be proposed. The minimum near $I = 25$, the gain in alignment larger than that associated with $(g_{9/2})^2$ configurations [Fig. 7(a)], and the positive parity of the states lead to the conclusion that band $D1$ must be associated with a configuration including three $g_{9/2}$ particles. From the calculations, an assignment to the $[31, 02]$ configuration is proposed, where the trajectory with signature $\alpha = -1/2$ for the five (fp) neutrons, $[31, 0(-)2]$, results in the best overall fit. The energy differences in the lower panel of Fig. 8 are rather constant for $I > 20$ at a value close to 1 MeV. The latter is somewhat high, but within acceptable limits for the calculations; see, e.g., Ref. [59]. With the method described in Ref. [61], an average transition quadrupole moment $Q_T = 1.7$ eb is calculated for this $[31, 0(-)2]$ configuration. However, a gradual migration of the local energy minimum for this configuration in the (β_2, γ) plane translates into the transition quadrupole moment decreasing from $\sim$1.9 eb at $I = 25/2$ to $\sim$1.5 eb for $I = 41/2$. The calculated Q_T value is about 30% lower than the experimental one, although the uncertainties on the latter are large. A similar observation has been made for other nuclei in this mass region (e.g., ^{59}Ni [39]).

TABLE II. Deformation parameters $|\beta_2|$ for selected bands in nuclei in the $A \approx 60$ mass region, compared to the parameters extracted for bands $D1$ and $D2$ in ^{63}Ni. Note that the parameters $|\beta_2|$ for ^{56}Ni, ^{58}Ni, and ^{60}Ni were inferred from comparisons of the available data with the results of cranked Nilsson-Strutinsky model calculations. The quoted calculated values represent an average over the spin ranges $I = 7$–19 (^{56}Ni), $I = 16$–32 (^{58}Ni), and $I = 11$–25 (^{60}Ni).

Nucleus	Band	$\lvert\beta_2\rvert$	Reference
^{56}Ni	$SD2$	0.34	[32,33]
^{57}Ni	$SD1$	$0.45^{+0.18}_{-0.14}$	[34]
^{58}Ni	$B3$	0.42	[37]
^{59}Ni	$B2$	0.29(9)	[39]
^{60}Ni	$WD2$	0.31	[41]
^{63}Ni	$D1$	$0.43^{+0.25}_{-0.20}$	this work
^{63}Ni	$D2$	$0.35^{+0.20}_{-0.21}$	this work
^{60}Zn	SD	0.47(7)	[53]
^{61}Zn	SD	$0.50^{+0.07}_{-0.06}$	[54]
^{62}Zn	$SD1$	$0.45^{+0.10}_{-0.07}$	[55,56]
^{65}Zn	$SD1$	0.43(5)	[52]

TABLE III. Nilsson parameters for $\mathcal{N} = 3$ and $\mathcal{N} = 4$ proton and neutron shells used in the present calculations.

		$\kappa_{\rm new}$	$\mu'_{\rm new}$
$\mathcal{N} = 3$	Protons	0.090	0.0370
	Neutrons	0.090	0.0325
$\mathcal{N} = 4$	Protons	0.0560	0.0319
	Neutrons	0.0804	0.0313

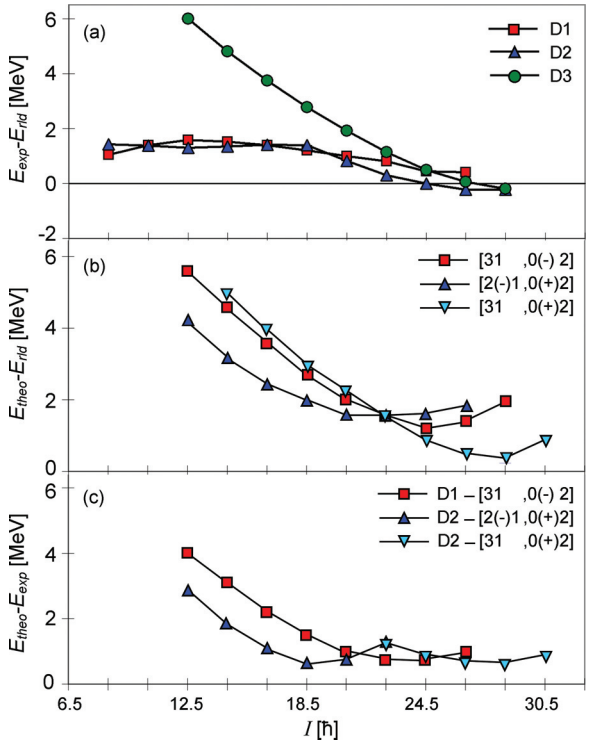

FIG. 8. (Color online) (a) Energies of the three observed deformed bands in ^{63}Ni drawn relative to a rotating liquid drop reference ($E_{\rm exp} - E_{\rm rld}$) as a function of spin I; (b) same as (a), but with energies calculated for the specific configurations indicated in the figure; (c) difference between calculated and experimental energies again plotted against I. See text for details.

In the I_x vs ω plot of Fig. 7(a), band $D2$ first exhibits a trajectory rather close to that of the $\nu(g_{9/2})^2$ configuration of ^{60}Fe before undergoing a band crossing around $\omega \sim 1.1$ MeV/$\hbar$, followed by a smooth increase in I_x mirroring that seen in band $D1$. The similarity between the two sequences at the highest frequencies suggests that they are associated with similar configurations, a finding supported by the results of the CNS calculations and a $[31, 0(+)2]$ assignment is proposed. This configuration differs from that proposed for band $D1$ by the signature of the three $f_{7/2}$ proton holes as well as that of the fp neutrons. As can be seen in Fig. 8, the agreement between the data and the calculations at high spin is comparable to that achieved in the case of band $D1$ with a difference between theory and data [panel (c)] of roughly 1 MeV. Most notably, the calculations predict this excitation to become yrast, in agreement with the data. Furthermore, the CNS results also indicate that this $[31, 0(+)2]$ configuration crosses the $[2(-)1, 0(+)2]$ one, resulting in the backbending seen in the data. Hence, the gain in alignment is understood in the CNS context as resulting from the single-particle crossing (unpaired crossing) involving the third $f_{7/2}$ orbital and the lowest fp state. It is interesting to note that the same crossing has been invoked earlier in the interpretation of bands $B1$ and $B2$ in ^{58}Ni [37,60]. In the case of ^{63}Ni, the crossing is calculated to occur at a spin of $I \approx 45/2$, a value somewhat higher than seen experimentally ($I \approx 37/2$) while, with the present parameters, the crossing is calculated at the correct spin value in ^{58}Ni [60].

In order to remove the discrepancy in ^{63}Ni, the $Z = 28$ gap would have to be decreased by $\sim$1 MeV, perhaps suggesting a decrease with increasing N in this $A = 60$ mass region. Nevertheless, the present interpretation should be viewed as tentative as, in addition to the difference in the spin value where the crossing occurs, the magnitude of the measured gain in alignment of $\sim 5\hbar$ is somewhat larger than the computed one of $\sim 3.5\hbar$. Finally, the CNS calculations yielded an average transition quadrupole moment of $Q_T = 1.5$ eb at the point where the two configurations of interest cross, consistent with the data within the large experimental errors and with the moment calculated for the $[31, 0(-)2]$ configuration of band $D1$. Just as was the case with the latter band, the Q_T moments for the two configurations associated with band $D2$ are calculated to decrease with increasing spin due to the migration of the local energy minima in the (β_2, γ) plane.

A configuration is not proposed for band $D3$ in view of the remaining uncertainties regarding the excitation energy, spin, and parity of its bandhead (see above). In Fig. 8(a), this sequence is presented under the assumptions used for Fig. 7(a); i.e., with an $E_x = 12.7$ MeV bandhead energy and a spin and parity of $25/2^-$. Under such a scenario, the $(E_{\rm exp} - E_{\rm rld})$ curve exhibits a behavior similar to those of bands $D1$ and $D2$ at higher spins ($I > 41/2$), supporting the suggestion of unobserved linking transitions between the band and the normally deformed states of structure $ND1$. In the CNS calculations, negative-parity configurations appear at energies close to those of the positive-parity ones. They involve the same proton orbitals, but require the excitation of an additional $g_{9/2}$ neutron. Such assignments are in line with the larger gain I_x exhibited by band $D3$ in Fig. 7(a). It should be noted that such configurations have been assigned to the high-spin bands in ^{65}Zn [52], for example. Additional measurements will be required to investigate such excitations further in ^{63}Ni.

C. Shell-model calculations of the $ND1$ level structure

The states regrouped under the $ND1$ label are built directly on the ground state and on the lowest levels which are understood as corresponding to excitations where the odd neutron occupies the various orbitals located near the Fermi surface. As the $ND1$ states do not exhibit the rotational characteristics of the $D1$, $D2$, and $D3$ bands, these are interpreted here in the framework of the shell model. For this purpose, calculations were performed with the Oslo shell-model code [62]. A ^{56}Ni core was assumed with a valence space restricted to the $f_{5/2}$, $p_{3/2}$, $p_{1/2}$, and $g_{9/2}$ neutron states. The JUN45 [63] and jj44b [64] effective interactions were considered.

The results of the calculations are compared with the data in Fig. 9. The comparison includes the $ND1$ states below 7.5 MeV and the bandheads of the two deformed bands $D1$ and $D2$ (marked in red in Fig. 9). A fair agreement between measured and calculated energies is achieved with either interaction with rms deviations of 0.49 MeV for the jj44b and 0.51 MeV for the JUN45 Hamiltonians, respectively. Note that these rms numbers deteriorate (0.60 MeV for jj44b and 0.53 MeV for JUN45) when the bandheads of the $D1$ and $D2$ bands are included, in line with expectations

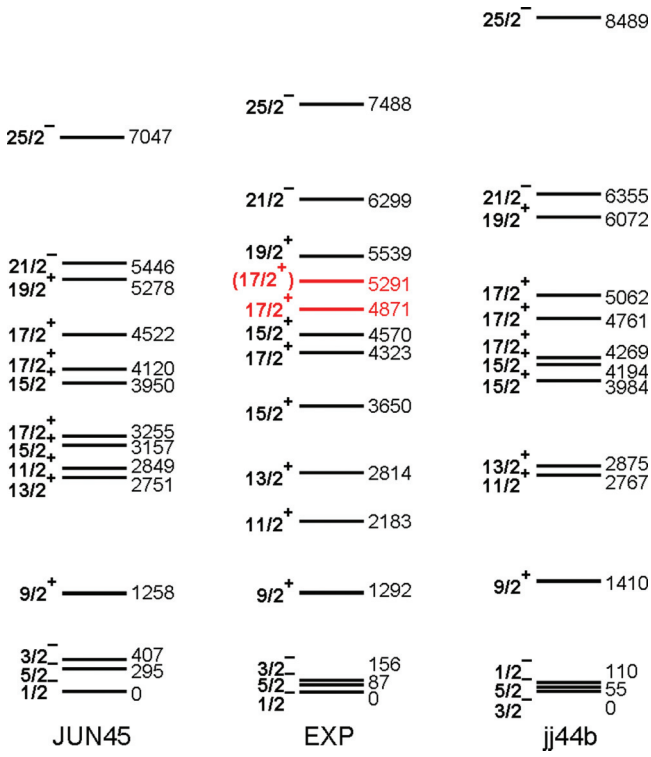

FIG. 9. (Color online) Experimental single-particle states in ^{63}Ni compared to shell-model calculations using the JUN45 and jj44b effective interactions. The bandheads of bands $D1$ and $D2$ are marked in red.

based on these two levels being associated with sizable deformation. The slightly lower rms deviation obtained with the jj44b Hamiltonian is not surprising since this interaction was obtained by including experimental data from nuclei with $Z = 28$ to 30 and $N = 48$ to 50 [64]. In contrast, the JUN45 effective interaction was derived by specifically excluding the Ni isotopes from the fit [63]. The jj44b interaction, however, fails to correctly reproduce the ground-state spin of $1/2^-$ [65], although the three lowest-lying states of spin and parity $3/2^-$, $5/2^-$, and $1/2^-$ are calculated to lie within a range of only 110 keV, reflecting the close proximity of the neutron single-particle orbitals $2p_{3/2}$, $1f_{5/2}$, and $2p_{1/2}$ in the ^{63}Ni nucleus. Finally, it is worth noting that both interactions predict the presence of rather closely-spaced pairs of states, such as the $11/2^+$–$13/2^+$ and $15/2^+$–$17/2^+$ sets, for example. Such pairs of levels have been observed recently in ^{67}Ni [31], but are less apparent in the $ND1$ structure. A more extensive study may be required to expand knowledge on the $ND1$ levels further. Alternatively, it is also possible that the available states exhibit a more vibrational-like character that would require a more expanded configuration space for an adequate description.

V. CONCLUSIONS

The level scheme of the semimagic nucleus ^{63}Ni has been extended up to an excitation energy of 28 MeV and a (tentative) spin and parity of $57/2^+$ with a novel experimental approach using complex reactions in inverse kinematics at energies roughly 200% above the Coulomb barrier. The residues of interest were identified in mass and charge through the FMA and the resolving power of Gammasphere enabled the use of a number of conventional spectroscopic techniques including high-fold coincidence studies, angular-distribution and -correlation measurements, and lifetime determinations by the Doppler-shift-attenuation method with thin targets. While the low-energy, low-spin level structure of ^{63}Ni exhibits properties characteristic of particle-hole excitations that can be understood with shell-model calculations, the higher-spin scheme is dominated by three rotational bands. For two of the three sequences, a sizable deformation was deduced, admittedly with large errors. Based on the results of cranked Nilsson-Strutinsky calculations, the two strongest excitations are understood as being associated with configurations involving multiple $f_{7/2}$ proton holes and $g_{9/2}$ neutrons which drive the nucleus to sizable deformation. These results extend the observation of collective motion in the Ni isotopic chain from ^{56}Ni and its neighbors to those midway to ^{68}Ni.

ACKNOWLEDGMENTS

The authors thank J. P. Greene (ANL) for target preparation and the ATLAS operations staff for the efficient running of the accelerator during the experiment. This work was supported in part by the U.S. Department of Energy, Office of Nuclear Physics, under Contract No. DE-AC02-06CH11357 and Grants No. DE-FG02-94ER40834 and No. DE-FG02-08ER41556, by the National Science Foundation under Contract No. PHY-0606007, by the Swedish Research Council, and by the United Kingdom Science and Technology Facilities Council (STFC).

[1] A. Gade, R. V. F. Janssens, D. Bazin, R. Broda, B. A. Brown, C. M. Campbell, M. P. Carpenter, J. M. Cook, A. N. Deacon, D.-C. Dinca, B. Fornal, S. J. Freeman, T. Glasmacher, P. G. Hansen, B. P. Kay, P. F. Mantica, W. F. Mueller, J. R. Terry, J. A. Tostevin, and S. Zhu, Phys. Rev. C **74**, 021302(R) (2006).

[2] R. V. F. Janssens, B. Fornal, P. F. Mantica, B. A. Brown, R. Broda, P. Bhattacharyya, M. P. Carpenter, M. Cinausero, P. J. Daly, A. D. Davies, T. Glasmacher, Z. W. Grabowski, D. E. Groh, M. Honma, F. G. Kondev, W. Królas, T. Lauritsen, S. N. Liddick, S. Lunardi, N. Marginean, T. Mizusaki, D. J. Morrissey, A. C. Morton, W. F. Mueller, T. Otsuka, T. Pawlat, D. Seweryniak, H. Schatz, A. Stolz, S. L. Tabor, C. A. Ur, G. Viesti, I. Wiedenhöver, and J. Wrzesinski, Phys. Lett. B **546**, 55 (2002).

[3] J. I. Prisciandaro, P. F. Mantica, B. A. Brown, D. W. Anthony, M. W. Cooper, A. Garcia, D. E. Groh, A. Komives, W. Kumarasiri, P. A. Lofy, A. M. Oros-Peusquens, S. L. Tabor, and M. Wiedeking, Phys. Lett. B **510**, 17 (2001).

[4] S. Zhu, A. N. Deacon, S. J. Freeman, R. V. F. Janssens, B. Fornal, M. Honma, F. R. Xu, R. Broda, I. R. Calderin, M. P. Carpenter, P. Chowdhury, F. G. Kondev, W. Królas, T. Lauritsen, S. N.

Liddick, C. J. Lister, P. F. Mantica, T. Pawłat, D. Seweryniak, J. F. Smith, S. L. Tabor, B. E. Tomlin, B. J. Varley, and J. Wrzesiński, Phys. Rev. C **74**, 064315 (2006).

[5] B. Fornal, S. Zhu, R. V. F. Janssens, M. Honma, R. Broda, P. F. Mantica, B. A. Brown, M. P. Carpenter, P. J. Daly, S. J. Freeman, Z. W. Grabowski, N. J. Hammond, F. G. Kondev, W. Królas, T. Lauritsen, S. N. Liddick, C. J. Lister, E. F. Moore, T. Otsuka, T. Pawłat, D. Seweryniak, B. E. Tomlin, and J. Wrzesiński, Phys. Rev. C **70**, 064304 (2004).

[6] D.-C. Dinca, R. V. F. Janssens, A. Gade, D. Bazin, R. Broda, B. A. Brown, C. M. Campbell, M. P. Carpenter, P. Chowdhury, J. M. Cook, A. N. Deacon, B. Fornal, S. J. Freeman, T. Glasmacher, M. Honma, F. G. Kondev, J.-L. Lecouey, S. N. Liddick, P. F. Mantica, W. F. Mueller, H. Olliver, T. Otsuka, J. R. Terry, B. A. Tomlin, and K. Yoneda, Phys. Rev. C **71**, 041302(R) (2005).

[7] A. Bürger, T. R. Saito, H. Grawe, H. Hübel, P. Reiter, J. Gerl, M. Gorska, H. J. Wollersheim, A. Al-Khatib, A. Banu, T. Beck, F. Becker, P. Bednarczyk, G. Benzoni, A. Bracco, S. Brambilla, P. Bringel, F. Camera, E. Clement, P. Doornenbal, H. Geissel, A. Görgen, J. Grebosz, G. Hammond, M. Hellström, M. Honma, M. Kavatsyuk, O. Kavatsyuk, M. Kmiecik, I. Kojouharov, W. Korten, N. Kurz, R. Lozeva, A. Maj, S. Mandal, B. Million, S. Muralithar, A. Neusser, F. Nowacki, T. Otsuka, Z. Podolyak, N. Saito, A. K. Singh, H. Weick, C. Wheldon, O. Wieland, and M. Winkler, Phys. Lett. B **622**, 29 (2005).

[8] D. Steppenbeck, S. Takeuchi, N. Aoi, P. Doornenbal, M. Matsushita, H. Wang, H. Baba, N. Fukuda, S. Go, M. Honma, J. Lee, K. Matsui, S. Michimasa, T. Motobayashi, D. Nishimura, T. Otsuka, H. Sakurai, Y. Shiga, P.-A. Söderström, T. Sumikama, H. Suzuki, R. Taniuchi, Y. Utsuno, J. J. Valiente-Dobón, and K. Yoneda, Nature (London) **502**, 207 (2013).

[9] T. Otsuka, R. Fujimoto, Y. Utsuno, B. A. Brown, M. Honma, and T. Mizusaki, Phys. Rev. Lett. **87**, 082502 (2001).

[10] T. Otsuka, T. Suzuki, R. Fujimoto, H. Grawe, and Y. Akaishi, Phys. Rev. Lett. **95**, 232502 (2005).

[11] T. Otsuka, T. Suzuki, M. Honma, Y. Utsuno, N. Tsunoda, K. Tsukiyama, and M. Hjorth-Jensen, Phys. Rev. Lett. **104**, 012501 (2010).

[12] T. Otsuka, Phys. Scr. T **152**, 014007 (2013) and references therein.

[13] A. Gade, R. V. F. Janssens, T. Baugher, D. Bazin, B. A. Brown, M. P. Carpenter, C. J. Chiara, A. N. Deacon, S. J. Freeman, G. F. Grinyer, C. R. Hoffman, B. P. Kay, F. G. Kondev, T. Lauritsen, S. McDaniel, K. Meierbachtol, A. Ratkiewicz, S. R. Stroberg, K. A. Walsh, D. Weisshaar, R. Winkler, and S. Zhu, Phys. Rev. C **81**, 051304(R) (2010).

[14] P. Adrich, A. M. Amthor, D. Bazin, M. D. Bowen, B. A. Brown, C. M. Campbell, J. M. Cook, A. Gade, D. Galaviz, T. Glasmacher, S. McDaniel, D. Miller, A. Obertelli, Y. Shimbara, K. P. Siwek, J. A. Tostevin, and D. Weisshaar, Phys. Rev. C **77**, 054306 (2008).

[15] T. Baugher, A. Gade, R. V. F. Janssens, S. M. Lenzi, D. Bazin, B. A. Brown, M. P. Carpenter, A. N. Deacon, S. J. Freeman, T. Glasmacher, G. F. Grinyer, F. G. Kondev, S. McDaniel, A. Poves, A. Ratkiewicz, E. A. McCutchan, D. K. Sharp, I. Stefanescu, K. A. Walsh, D. Weisshaar, and S. Zhu, Phys. Rev. C **86**, 011305(R) (2012).

[16] H. L. Crawford, R. M. Clark, P. Fallon, A. O. Macchiavelli, T. Baugher, D. Bazin, C. W. Beausang, J. S. Berryman, D. L. Bleuel, C. M. Campbell, M. Cromaz, G. de Angelis, A. Gade, R. O. Hughes, I. Y. Lee, S. M. Lenzi, F. Nowacki, S. Paschalis, M. Petri, A. Poves, A. Ratkiewicz, T. J. Ross, E. Sahin, D. Weisshaar, K. Wimmer, and R. Winkler, Phys. Rev. Lett. **110**, 242701 (2013).

[17] J. Ljungvall, A. Görgen, A. Obertelli, W. Korten, E. Clément, G. de France, A. Bürger, J.-P. Delaroche, A. Dewald, A. Gadea, L. Gaudefroy, M. Girod, M. Hackstein, J. Libert, D. Mengoni, F. Nowacki, T. Pissulla, A. Poves, F. Recchia, M. Rejmund, W. Rother, E. Sahin, C. Schmitt, A. Shrivastava, K. Sieja, J. J. Valiente-Dobón, K. O. Zell, and M. Zielińska, Phys. Rev. C **81**, 061301 (2010).

[18] N. Hoteling, C. J. Chiara, R. Broda, W. B. Walters, R. V. F. Janssens, M. Hjorth-Jensen, M. P. Carpenter, B. Fornal, A. A. Hecht, W. Królas, T. Lauritsen, T. Pawłat, D. Seweryniak, X. Wang, A. Wöhr, J. Wrzesiński, and S. Zhu, Phys. Rev. C **82**, 044305 (2010).

[19] A. N. Deacon, S. J. Freeman, R. V. F. Janssens, F. R. Xu, M. P. Carpenter, I. R. Calderin, P. Chowdhury, N. J. Hammond, T. Lauritsen, C. J. Lister, D. Seweryniak, J. F. Smith, S. L. Tabor, B. J. Varley, and S. Zhu, Phys. Lett. B **622**, 151 (2005).

[20] N. Hoteling, W. B. Walters, R. V. F. Janssens, R. Broda, M. P. Carpenter, B. Fornal, A. A. Hecht, M. Hjorth-Jensen, W. Królas, T. Lauritsen, T. Pawłat, D. Seweryniak, X. Wang, A. Wöhr, J. Wrzesiński, and S. Zhu, Phys. Rev. C **74**, 064313 (2006).

[21] A. N. Deacon, S. J. Freeman, R. V. F. Janssens, M. Honma, M. P. Carpenter, P. Chowdhury, T. Lauritsen, C. J. Lister, D. Seweryniak, J. F. Smith, S. L. Tabor, B. J. Varley, F. R. Xu, and S. Zhu, Phys. Rev. C **76**, 054303 (2007).

[22] D. Steppenbeck, R. V. F. Janssens, S. J. Freeman, M. P. Carpenter, P. Chowdhury, A. N. Deacon, M. Honma, H. Jin, T. Lauritsen, C. J. Lister, J. Meng, J. Peng, D. Seweryniak, J. F. Smith, Y. Sun, S. L. Tabor, B. J. Varley, Y.-C. Yang, S. Q. Zhang, P. W. Zhao, and S. Zhu, Phys. Rev. C **85**, 044316 (2012).

[23] M. P. Carpenter, R. V. F. Janssens, and S. Zhu, Phys. Rev. C **87**, 041305(R) (2013).

[24] S. M. Lenzi, F. Nowacki, A. Poves, and K. Sieja, Phys. Rev. C **82**, 054301 (2010).

[25] K. Sieja and F. Nowacki, Phys. Rev. C **85**, 051301 (2012).

[26] R. Broda, T. Pawłat, W. Królas, R. V. F. Janssens, S. Zhu, W. B. Walters, B. Fornal, C. J. Chiara, M. P. Carpenter, N. Hoteling, Ł. W. Iskra, F. G. Kondev, T. Lauritsen, D. Seweryniak, I. Stefanescu, X. Wang, and J. Wrzesiński, Phys. Rev. C **86**, 064312 (2012) and references therein.

[27] J. P. Schiffer, C. R. Hoffman, B. P. Kay, J. A. Clark, C. M. Deibel, S. J. Freeman, M. Honma, A. M. Howard, A. J. Mitchell, T. Otsuka, P. D. Parker, D. K. Sharp, and J. S. Thomas, Phys. Rev. C **87**, 034306 (2013).

[28] M. Bernas, P. Dessagne, M. Langevin, J. Payet, F. Pougheon, and P. Roussel, Phys. Lett. B **113**, 279 (1982).

[29] O. Sorlin, S. Leenhardt, C. Donzaud, J. Duprat, F. Azaiez, F. Nowacki, H. Grawe, Z. Dombrádi, F. Amorini, A. Astier, D. Baiborodin, M. Belleguic, C. Borcea, C. Bourgeois, D. M. Cullen, Z. Dlouhy, E. Dragulescu, M. Górska, S. Grévy, D. Guillemaud-Mueller, G. Hagemann, B. Herskind, J. Kiener, R. Lemmon, M. Lewitowicz, S. M. Lukyanov, P. Mayet, F. de Oliveira Santos, D. Pantalica, Y.-E. Penionzhkevich, F. Pougheon, A. Poves, N. Redon, M. G. Saint-Laurent, J. A. Scarpaci, G. Sletten, M. Stanoiu, O. Tarasov, and C. Theisen, Phys. Rev. Lett. **88**, 092501 (2002).

[30] R. Broda, B. Fornal, W. Królas, T. Pawłat, D. Bazzacco, S. Lunardi, C. Rossi-Alvarez, R. Menegazzo, G. de Angelis,

P. Bednarczyk, J. Rico, D. De Acuña, P. J. Daly, R. H. Mayer, M. Sferrazza, H. Grawe, K. H. Maier, and R. Schubart, Phys. Rev. Lett. **74**, 868 (1995).

[31] S. Zhu, R. V. F. Janssens, M. P. Carpenter, C. J. Chiara, R. Broda, B. Fornal, N. Hoteling, W. Królas, T. Lauritsen, T. Pawłat, D. Seweryniak, I. Stefanescu, J. R. Stone, W. B. Walters, X. Wang, and J. Wrzesiński, Phys. Rev. C **85**, 034336 (2012).

[32] D. Rudolph, C. Baktash, M. J. Brinkman, E. Caurier, D. J. Dean, M. Devlin, J. Dobaczewski, P.-H. Heenen, H.-Q. Jin, D. R. LaFosse, W. Nazarewicz, F. Nowacki, A. Poves, L. L. Riedinger, D. G. Sarantites, W. Satuła, and C.-H. Yu, Phys. Rev. Lett. **82**, 3763 (1999).

[33] E. K. Johansson, D. Rudolph, L.-L. Andersson, D. A. Torres, I. Ragnarsson, C. Andreoiu, C. Baktash, M. P. Carpenter, R. J. Charity, C. J. Chiara, J. Ekman, C. Fahlander, C. Hoel, O. L. Pechenaya, W. Reviol, R. du Rietz, D. G. Sarantites, D. Seweryniak, L. G. Sobotka, C. H. Yu, and S. Zhu, Phys. Rev. C **77**, 064316 (2008).

[34] W. Reviol, D. Sarantites, R. Charity, V. Tomov, D. Rudolph, R. Clark, M. Cromaz, P. Fallon, A. Macchiavelli, M. Carpenter, D. Seweryniak, and J. Dobaczewski, Nucl. Phys. A **682**, 28c (2001).

[35] D. Rudolph, I. Ragnarsson, W. Reviol, C. Andreoiu, M. A. Bentley, M. P. Carpenter, R. J. Charity, R. M. Clark, M. Cromaz, J. Ekman, C. Fahlander, P. Fallon, E. Ideguchi, A. O. Macchiavelli, M. N. Mineva, D. G. Sarantites, D. Seweryniak, and S. J. Williams, J. Phys. G: Nucl. Part. Phys. **37**, 075105 (2010).

[36] D. Rudolph, C. Baktash, M. Devlin, D. R. LaFosse, L. L. Riedinger, D. G. Sarantites, and C.-H. Yu, Phys. Rev. Lett. **86**, 1450 (2001).

[37] D. Rudolph, B. G. Carlsson, I. Ragnarsson, S. Åberg, C. Andreoiu, M. A. Bentley, M. P. Carpenter, R. J. Charity, R. M. Clark, M. Cromaz, J. Ekman, C. Fahlander, P. Fallon, E. Ideguchi, A. O. Macchiavelli, M. N. Mineva, W. Reviol, D. G. Sarantites, D. Seweryniak, and S. J. Williams, Phys. Rev. Lett. **96**, 092501 (2006).

[38] E. K. Johansson, D. Rudolph, I. Ragnarsson, L.-L. Andersson, D. A. Torres, C. Andreoiu, C. Baktash, M. P. Carpenter, R. J. Charity, C. J. Chiara, J. Ekman, C. Fahlander, O. L. Pechenaya, W. Reviol, R. du Rietz, D. G. Sarantites, D. Seweryniak, L. G. Sobotka, C. H. Yu, and S. Zhu, Phys. Rev. C **80**, 014321 (2009).

[39] C.-H. Yu, C. Baktash, J. A. Cameron, M. Devlin, J. Eberth, A. Galindo-Uribarri, D. S. Haslip, D. R. LaFosse, T. J. Lampman, I.-Y. Lee, F. Lerma, A. O. Macchiavelli, S. D. Paul, D. C. Radford, I. Ragnarsson, D. Rudolph, D. G. Sarantites, C. E. Svensson, J. C. Waddington, J. C. Wells, and J. N. Wilson, Phys. Rev. C **65**, 061302(R) (2002).

[40] D. Cutoiu, S. Juutinen, S. E. Arnell, P. Ahonen, M. Bentley, B. Cederwall, A. Johnson, B. Fant, R. Julin, S. Mitarai, J. Mukai, J. Nyberg, H. Roth, O. Skeppstedt, S. Tormanen, and A. Virtanen, JYFL Annual Report 1991 (unpublished), p.58.

[41] D. A. Torres, F. Cristancho, L.-L. Andersson, E. K. Johansson, D. Rudolph, C. Fahlander, J. Ekman, R. du Rietz, C. Andreoiu, M. P. Carpenter, D. Seweryniak, S. Zhu, R. J. Charity, C. J. Chiara, C. Hoel, O. L. Pechenaya, W. Reviol, D. G. Sarantites, L. G. Sobotka, C. Baktash, C.-H. Yu, B. G. Carlsson, and I. Ragnarsson, Phys. Rev. C **78**, 054318 (2008).

[42] E. K. Warburton, J. W. Olness, A. M. Nathan, and A. R. Poletti, Phys. Rev. C **18**, 1637 (1978).

[43] B. Erjun and H. Junde, Nucl. Data Sheets **92**, 147 (2001).

[44] R. Broda, J. Phys. G: Nucl. Part. Phys. **32**, R151 (2006).

[45] I. Y. Lee, Nucl. Phys. A **520**, 641c (1990).

[46] C. N. Davids, B. B. Back, K. Bindra, D. J. Henderson, W. Kutschera, T. Lauritsen, Y. Nagame, P. Sugathan, A. V. Ramayya, and W. B. Walters, Nucl. Instrum. Methods Phys. Res. Sect. B **70**, 358 (1992).

[47] T. Yamazaki, Nucl. Data Sec. A **3**, 1 (1967).

[48] K. S. Krane, R. M. Steffen, and R. M. Wheeler, At. Data and Nucl. Data Tables **11**, 351 (1973).

[49] B. Cederwall, I. Y. Lee, S. Asztalos, M. J. Brinkman, J. A. Becker, R. M. Clark, M. A. Deleplanque, R. M. Diamond, P. Fallon, L. P. Farris, E. A. Henry, J. R. Hughes, A. O. Macchiavelli, and F. S. Stephens, Nucl. Instrum. Meth. Phys. Res. A **354**, 591 (1995).

[50] E. F. Moore, T. Lauritsen, R. V. F. Janssens, T. L. Khoo, D. Ackermann, I. Ahmad, H. Amro, D. Blumenthal, M. P. Carpenter, S. M. Fischer, G. Hackman, D. Nisius, F. Hannachi, A. Lopez-Martens, A. Korichi, S. Asztalos, R. M. Clark, M. A. Deleplanque, R. M. Diamond, P. Fallon, I. Y. Lee, A. O. Macchiavelli, F. S. Stephens, J. A. Becker, L. Bernstein, L. P. Farris, and E. A. Henry, Phys. Rev. C **55**, R2150 (1997).

[51] J. F. Ziegler, J. P. Biersack, and U. Littmark, *The Stopping and Range of Ions in Solids* (Pergamon, New York, 1985).

[52] C.-H. Yu, C. Baktash, J. Dobaczewski, J. A. Cameron, M. Devlin, J. Eberth, A. Galindo-Uribarri, D. S. Haslip, D. R. LaFosse, T. J. Lampman, I.-Y. Lee, F. Lerma, A. O. Macchiavelli, S. D. Paul, D. C. Radford, D. Rudolph, D. G. Sarantites, C. E. Svensson, J. C. Waddington, and J. N. Wilson, Phys. Rev. C **62**, 041301 (2000).

[53] C. E. Svensson, D. Rudolph, C. Baktash, M. A. Bentley, J. A. Cameron, M. P. Carpenter, M. Devlin, J. Eberth, S. Flibotte, A. Galindo-Uribarri, G. Hackman, D. S. Haslip, R. V. F. Janssens, D. R. LaFosse, T. J. Lampman, I. Y. Lee, F. Lerma, A. O. Macchiavelli, J. M. Nieminen, S. D. Paul, D. C. Radford, P. Reiter, L. L. Riedinger, D. G. Sarantites, B. Schaly, D. Seweryniak, O. Thelen, H. G. Thomas, J. C. Waddington, D. Ward, W. Weintraub, J. N. Wilson, C. H. Yu, A. V. Afanasjev, and I. Ragnarsson, Phys. Rev. Lett. **82**, 3400 (1999).

[54] C.-H. Yu, C. Baktash, J. Dobaczewski, J. A. Cameron, C. Chitu, M. Devlin, J. Eberth, A. Galindo-Uribarri, D. S. Haslip, D. R. LaFosse, T. J. Lampman, I.-Y. Lee, F. Lerma, A. O. Macchiavelli, S. D. Paul, D. C. Radford, D. Rudolph, D. G. Sarantites, C. E. Svensson, J. C. Waddington, and J. N. Wilson, Phys. Rev. C **60**, 031305(R) (1999).

[55] C. E. Svensson, C. Baktash, J. A. Cameron, M. Devlin, J. Eberth, S. Flibotte, D. S. Haslip, D. R. LaFosse, I. Y. Lee, A. O. Macchiavelli, R. W. MacLeod, J. M. Nieminen, S. D. Paul, L. L. Riedinger, D. Rudolph, D. G. Sarantites, H. G. Thomas, J. C. Waddington, W. Weintraub, J. N. Wilson, A. V. Afanasjev, and I. Ragnarsson, Phys. Rev. Lett. **79**, 1233 (1997).

[56] J. Gellanki, I. Ragnarsson, D. Rudolph, C. E. Svensson, L. L. Andersson, C. Andreoiu, C. Baktash, M. P. Carpenter, R. J. Charity, C. J. Chiara, J. Eberth, J. Ekman, C. Fahlander, D. S. Haslip, E. K. Johansson, D. R. LaFosse, S. D. Paul, O. L. Pechenaya, W. Reviol, R. du Rietz, D. G. Sarantites, D. Seweryniak, L. G. Sobotka, H. G. Thomas, D. A. Torres, J. C. Waddington, J. N. Wilson, C. H. Yu, and S. Zhu, Phys. Rev. C **80**, 051304(R) (2009).

[57] T. Bengtsson and I. Ragnarsson, Nucl. Phys. A **436**, 14 (1985).

[58] A. V. Afanasjev, D. B. Fossan, G. J. Lane, and I. Ragnarsson, Phys. Rep. **322**, 1 (1999).
[59] B. G. Carlsson and I. Ragnarsson, Phys. Rev. C **74**, 011302(R) (2006).
[60] J. Gellanki *et al*. (unpublished).
[61] X. Wang, M. A. Riley, J. Simpson, E. S. Paul, J. Ollier, R. V. F. Janssens, A. D. Ayangeakaa, H. C. Boston, M. P. Carpenter, C. J. Chiara, U. Garg, D. J. Hartley, D. S. Judson, F. G. Kondev, T. Lauritsen, N. M. Lumley, J. Matta, P. J. Nolan, M. Petri, J. P. Revill, L. L. Riedinger, S. V. Rigby, C. Unsworth, S. Zhu, and I. Ragnarsson, Phys. Lett. B **702**, 127 (2011).
[62] M. Hjorth-Jensen, T. T. S. Kuo, and E. Osnes, Phys. Rep. **261**, 125 (1995).
[63] M. Honma, T. Otsuka, T. Mizusaki, and M. Hjorth-Jensen, Phys. Rev. C **80**, 064323 (2009).
[64] B. A. Brown (private communication); see also Ref. [28] in B. Cheal *et al*., Phys. Rev. Lett. **104**, 252502 (2010).
[65] R. H. Fulmer and A. L. McCarthy, Phys. Rev. **131**, 2133 (1963).